Aerosol and Air Quality Research, 18: 1799–1816, 2018

ISSN: 1680-8584 print / 2071-1409 online
doi: 10.4209/aaqr.2017.09.0322

Effects of Wintertime Polluted Aerosol on Clouds over the Yangtze River Delta: Case Study

Chen Xu[1], Junyan Duan[1], Yanyu Wang[1], Mei Li[2], Tiantao Cheng[1*], Hua Wang[3*], Hailin Zhu[1], Xin Xie[1], Yuehui Liu[1], Yan Ling[1], Xiang Li[1], Lingdong Kong[1], Qianshan He[4], Hongli Wang[5], Renjian Zhang[6]

[1] *Shanghai Key Laboratory of Atmospheric Particle Pollution and Prevention (LAP[3]), Department of Environmental Science and Engineering, Institute of Atmospheric Sciences, Fudan University, Shanghai 200433, China*
[2] *Guangdong Engineering Research Center for Online Atmospheric Pollution Source Apportionment Mass Spectrometry System, Institute of Mass Spectrometer and Atmospheric Environment, Jinan University, Guangzhou 510632, China*
[3] *Environmental and Meteorology Forecast Center of Beijing-Tianjin-Hebei, Beijing 100089, China*
[4] *Shanghai Meteorological Bureau, Shanghai 20030, China*
[5] *State Environmental Protection Key Laboratory of Formation and Prevention of Urban Air Pollution Complex, Institute of Atmospheric Environment, Shanghai Academy of Environmental Sciences, Shanghai 200233, China*
[6] *Key Laboratory of Region Climate-Environment Research for Temperate East Asia (CAS-TEA), Institute of Atmospheric Physics, Chinese Academy of Sciences, Beijing 100029, China*

ABSTRACT

The effects of aerosol on clouds are examined over the Yangtze River Delta (YRD) using 3 months of satellite data from the polluted wintertime from December 2013 to February 2014. The relationships between aerosol properties, and cloud micro- and macro-physical parameters are analyzed in detail to clarify the differences in cloud development under various aerosol and meteorological conditions. Complex relationships between the aerosol optical depth (AOD), and the cloud droplet radius (CDR), liquid water path (LWP) and cloud optical thickness (COT) exist in four regions of interest (ROIs). High aerosol loading does not obviously affect LWPs and COTs; in fact, aerosols inhibit development of low- and medium-low clouds over coastal areas—an effect that is more pronounced in low clouds (< 5 km) than high ones. Low aerosol loading plays a positive role in promoting the COT of high- and low-clouds over areas dominated by maritime aerosol. Aerosol loading exerts a significant influence on COTs, LWPs and CDRs in valley and coal industry districts except during high-cloud conditions. The ranges of COTs, LWPs and CDRs in dry-polluted areas are lower than in other places, which suggests that dust aerosol has little effect on cloud properties. Synoptic conditions also strongly impact cloud distribution, in particular, an unstable synoptic condition leads to cloud development on a larger horizontal and vertical scale. Ground pollution enhances the amount of low-level cloud cover even under stable conditions. Aerosol plays an important role in wintertime cloud evolution in the low layers of the troposphere (< 5 km) when the atmosphere is stable.

Keywords: Aerosol; Cloud; Pollution; The Yangtze River Delta.

INTRODUCTION

Aerosols are solid or liquid particles with diameters of 0.001–10 microns suspended in the atmosphere. Aerosol can influence regional and global climates by direct and indirect effects (Ackerman *et al.*, 2000; Forest *et al.*, 2002; Knutti *et al.*, 2002; Anderson *et al.*, 2003; Lohmann and Feichter, 2005; Satheesh *et al.*, 2006), and causes great harm to atmospheric environment and human health (Pöschl, 2005; Monks *et al.*, 2009). Aerosol can act as cloud condensation nuclei (CCN) or ice nuclei (IN) to affect cloud droplet size, number and albedo, and as a result, delay cloud droplet growth by collision and coalescence in warm clouds (Twomey, 1974). Aerosol also affects precipitation and cloud lifetime, thus eventually affect cloud coverage and regional climate (Albrecht, 1989; Rosenfeld, 2000; Ramanathan *et al.*, 2001; Quaas *et al.*, 2004). In the process of cloud formation, aerosol probably influences cloud physical characteristics, such as cloud thickness and cloud

* Corresponding author.
Tel: (86) 21-6564 3230; Fax: (86) 21-6564 2080
E-mail address: ttcheng@fudan.edu.cn;
huawang0707@sina.com

amount (Hansen *et al.*, 1997).

The Yangtze River Delta (YRD) is an economic fast-growing and densely populated area in East China. Due to human activities, this region suffers substantially from increasing anthropogenic aerosols over the last decades (Wolf and Hidy, 1997; Streets *et al.*, 2001; Xu *et al.*, 2003; Bond *et al.*, 2004; Lu *et al.*, 2010). Other types of aerosols present in the YRD are marine aerosol from sea surface brought by winds, and dust transported occasionally from deserts in northern China mostly in winter and spring (Jin and Shepherd, 2008). All these factors may result in a more complex aerosol-cloud-precipitation interaction over this region.

In recent years, increasing attention has been paid to aerosol and its radiative effect in the YRD district (Xia *et al.*, 2007; Liu *et al.*, 2012). He *et al.* (2012) revealed a notable increase in annual mean aerosol optical depth (AOD) during 2000–2007, with a maximum in summer dominated by fine particles and a minimum in winter controlled mostly by coarse particles. Other studies have focused on the aerosol indirect effect (AIE) in an attempt to assess the impact of aerosol on precipitation in East China. For example, Leng *et al.* (2014) pointed out that particles are more active as CCN during hazy days in Shanghai. Tang *et al.* (2014) analyzed the variability of cloud properties induced by aerosol over East China from satellite data, and compared land with ocean areas to understand AIE discrepancies under different meteorological conditions. Menon *et al.* (2002) proposed that South China Flood–North China Drought patterns caused by anthropogenic aerosol are likely attributable to the radiative absorption by black carbon aerosols. Zhao *et al.* (2006) examined the positive feedback of precipitation on aerosol over eastern and central China for the last 40 years, and revealed that precipitation has significantly decreased in conjunction with a reduction in atmospheric visibility. The decreases in the frequency of afternoon-to-evening local-scale precipitation are reportedly associated with increases in aerosol pollution in eastern China (Guo *et al.*, 2017). Based on multi-satellite observations, the response of the effective radius of warm cloud droplets (Reff) to aerosol was found to exhibit a boomerang shape, that is to say, Reff tends to decrease as the atmosphere becomes slightly polluted, and this reverses to yield a Reff increase after the aerosol exceeds some threshold value (Wang *et al.*, 2015). Despite the advances made by the above-mentioned studies, up to now, the influence of polluted aerosol on cloud and precipitation over the different underlying surfaces of the YRD has not been intensively examined.

In the winter of 2013, China was extensively affected by heavy pollution (e.g., haze), which was characterized by long-term durability, wide influence and severe pollution features. In the YRD, air pollution episodes occurred persistently from December 2013 to February 2014. Leng *et al.* (2016) analyzed the synoptic situation, boundary layer and pollutants of the haze that occurred in December 2013, and Hu *et al.* (2016) outlined the chemical characteristics of single particles sampled in Shanghai. Kong *et al.* (2015) observed the variation of polycyclic aromatic hydrocarbons in $PM_{2.5}$ during haze periods around the 2014 Chinese Spring Festival in Nanjing. However, more efforts are needed to focus on the relationship between aerosol and cloud macro-/micro-physical properties under different atmospheric conditions.

This paper presents the spatio-temporal variations of aerosol and clouds over the YRD region from December 2013 to February 2014 using satellite retrieval products. We first focus on the relationships between aerosol and cloud microphysical properties, including AODs-COTs, AODs-LWPs, AODs-CDRs. We then investigate how aerosol (aerosol loading and types) affects the vertical and fractional distribution of cloud. Finally, in a 4-day case study of polluted aerosol and cloud development, we take aerosol type, cloud microphysical proprieties (COT, CDR, LWP), cloud fraction and the synoptic system into account to make a detailed study of the aerosol indirect effect during a polluted period. The aim is to provide insights into the influence of aerosol on cloud micro- and macro-physical properties under highly polluted conditions. The results are helpful to improve in-depth understanding of aerosol indirect effects over fast-growing Asian areas.

DATA AND METHODS

The Clouds and Earth's Radiant Energy System (CERES), a part of the NASA's Earth Observing System (EOS), is an instrument on board the Aqua satellite that measures the upwelling short- and long-wave radiation with a horizontal resolution of about 20 × 20 km^2 (Wielicki *et al.*, 1996; Loeb and Manalo-Smith, 2005). In this study, the cloud and aerosol parameters of CERES-SYN (Edition 3A) 3-hour data from Terra and Aqua, are used for the YRD domain (26.5–35.5°N, 115.5–122.5°E) between December 2013 and February 2014. Cloud properties, including liquid water path (LWP), cloud droplet effective radius (CDR), cloud optical thickness (COT), cloud top pressure (CTP) and cloud fraction (CF), are retrieved from the 3.7 μm (mid-IR) channel with a horizontal resolution of 1° × 1° (Minnis *et al.*, 2004). A daily average is computed from several 3-hour data corresponding to the date of SYN products. On the basis of the 3-month mean AOD (0.55 μm) and underlying surface conditions, the YRD is divided into four ROIs (Fig. 1).

The CERES-SYN retrieval includes MODIS-derived cloud and aerosol properties (Minnis *et al.*, 2004; Remer *et al.*, 2005) and geostationary-derived cloud properties. It uses 3-hour cloud property data from geostationary (GEO) imagers for modelling more accurately the variability of CERES observations. Computations use MODIS and GEO satellite cloud properties along with atmospheric profiles provided by the Global Modeling and Assimilation Office (GMAO). Furthermore, the CDR and COT of MOD04 are generally smaller than the MOD06 products (Platnick *et al.*, 2003; Minnis *et al.*, 2004) because the MODIS algorithm of MOD04 tends to classify very thick aerosol layers as cloud and non-aerosol (Remer *et al.*, 2006). Thus, the total AOD is probably underestimated by MODIS. Overall, the properties of cloud and aerosol are more accurately retrieved from the CERES-SYN (Jones *et al.*, 2009).

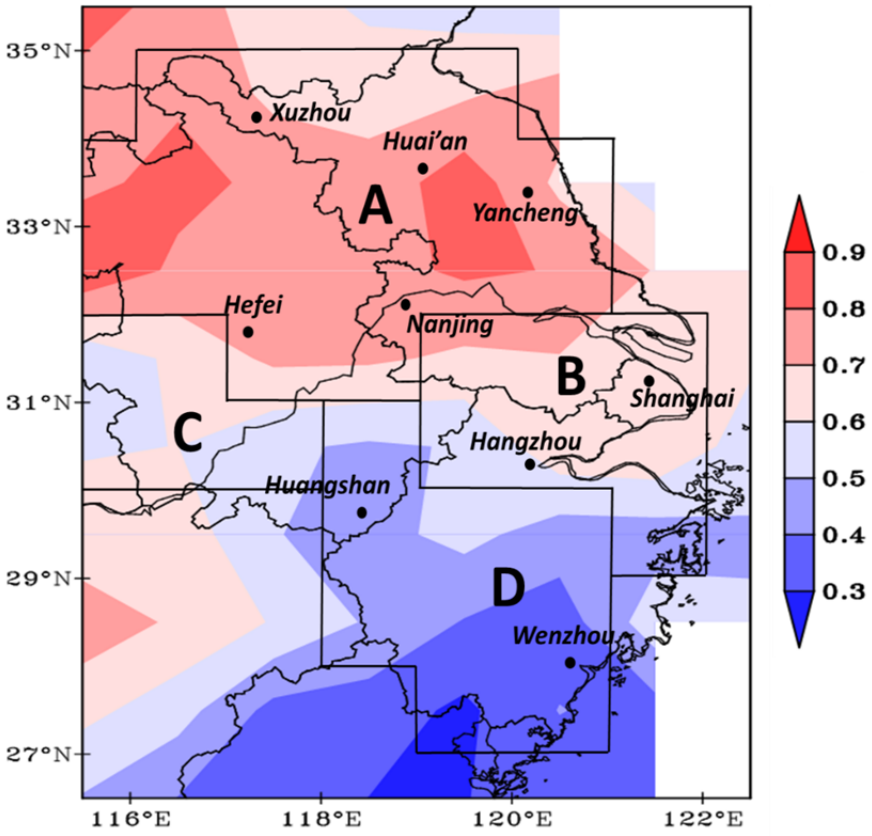

Fig. 1. Three-monthly mean aerosol optical depth (AOD) at 0.55 μm over the Yangtze River Delta (YRD) from CERES-SYN between December 2013 and February 2014. The major cities in this region and four regions of interest (ROIs): ROI-A, ROI-B, ROI-C, ROI-D and their borders (black lines on the map), which are marked.

MODIS products are derived from cloud-free data at 500-m spatial resolution and then aggregated to a 10-km footprint (20 × 20 pixels) to generate the Level 2 aerosol product (MOD04). In this study, a simple method (Barnaba and Gobbi, 2004), based on the combination of AOD and the fine mode fraction (FMF) at 0.55 μm, is implemented to determine aerosol types. Aerosol is defined as marine type when AOD < 0.3 and FMF < 0.8, dust when AOD > 0.3 and FMF < 0.7, and continental type when AOD < 0.3 and FMF > 0.8 or AOD > 0.3 and FMF > 0.7.

The vertical feature of aerosol and cloud is characterized using the retrieval from CALIPSO, which provides height-resolved information globally since 2006, including the layer fraction of aerosol and cloud and aerosol vertical feature mask (Winker *et al.*, 2009, 2010). In addition, surface lifted index (SLI) and sea level pressure (SLP) from the National Center for Environmental Prediction (NCEP) Reanalysis (Kalnay *et al.*, 1996) are used to examine atmospheric stability. The frequency of precipitation is calculated using the precipitation rate from the NCEP reanalysis data.

The Hybrid Single Particle Lagrangian Integrated Trajectory (HYSPLIT) model (Draxler and Rolph 2003; Rolph 2003; www.arl.noaa.gov/ready.html) is used to calculate 72-h air mass forward- and backward trajectories every six hours at 9 key sites of the YRD. The meteorological input is from the FNL data set, reprocessed from the final analysis data by Air Resources Laboratory. Finally, the study also analyses observational data of $PM_{2.5}$ concentration obtained from the on-line monitoring and analysis platform of air quality in China (http://www.aqistudy.cn/). Herein, Table 1 lists all the aerosol and cloud parameters used in this study.

RESULTS AND DISCUSSION

Aerosol Spatial Distribution

Fig. 1 displays the spatial distribution of 3-h mean AODs over the YRD between December 2013 and February 2014. The range of AODs is 0.3–0.9, lower than the annual average (0.5–1.3) (Kourtidis *et al.*, 2015), and the AODs show a significant distinction depending on the different surface conditions from north to south. High AODs are mostly found in plains and valleys, particularly over the densely populated and industrialized locations, while low AODs are mainly distributed in the hills and mountains. AODs higher than 0.7 are concentrated in the north of the YRD, the central and northern parts of Jiangsu Province and the northern part of Anhui Province, traditional agricultural areas, which are here defined as the ROI-A. Furthermore, high AODs of 0.5–0.7 are found in Shanghai and the northeastern part of Zhejiang Province, typical urban industrial areas, named ROI-B. The Yangtze River valley in Anhui Province, surrounded by Dabie and Tianmu Mountains, is categorized as the ROI-C. The Dabie and Tianmu Mountains may prevent

Table 1. Details of parameters, which are used in our study.

Parameters	Products	Algorithm & Source	Satellites Channel	Resolution
AOD, FMF	CERES-SYN Edition 3A 3-hour	MODIS-derived (MOD04)	Terra and Aqua 0.55 μm	1° × 1° (horizontal)
COT, LWP,CTP, CLF, CDR		MODIS-Geostationary (3-hour)-derived	3.7 μm (mid-IR)	
Aerosol layer fraction	CAL_LID_L2_05kmAPro-Prov-V3-30	CALIOP lidar-GMAO	CALIPSO	5 km (horizontal)
cloud layer fraction				60 m (Vertical)
Aerosol vertical feature mask	CAL_LID_L2_VFM-ValStage1-V3-30			5 km (horizontal)
				30 m (Vertical)
SLI, SLP, precipitation rate	National Center for Environmental Prediction (NCEP) Reanalysis			2.5° × 2.5° (horizontal)
Air mass trajectories	HYSPLIT model			Every 6 hours at 9 key sites
$PM_{2.5}$ concentration		Air quality network in China		Daily average

the long-distance transportation of dust and anthropogenic aerosol from the northwest and marine salt from the southeast, respectively. AODs lower than 0.5 are observed in mountainous areas throughout the south and the west part of Zhejiang Province and Mount Huang in Anhui Province, referred to as the ROI-D.

The 3-month mean AODs are 0.76, 0.62, 0.57 and 0.44 in the ROI-A, ROI-B, ROI-C and ROI-D, respectively. This feature of aerosol spatial distribution is in accordance with the result of Tan *et al.* (2015) concluded using 10-year data, that aerosol concentration is higher in the north and lower in the south, whereas FMF exhibits the opposite trend to AOD.

According to the AOD~FMF classification method (Barnaba and Gobbi,2004), aerosols of the ROI-A are most likely categorized into marine, dust and continental types, mainly generated from local urban/industrial emissions and biomass burning. Also, ROI-A is vulnerable to dust advection from Northern China (Fu *et al.*, 2014). In the ROI-B, besides fine mode particles from urban/industrial emissions, coarse mode particulate pollutants include marine aerosols due to the humidity swelling of sea salt (Xin *et al.*, 2007) brought by northeastern airflows and dust transported over long distances from the north. Many construction and industrial activities also contribute numerous dust-like particles to the atmosphere (He *et al.*, 2012). Similar to the aerosol types in the ROI-B, the ROI-C is home to more than one million people, numerous copper-melting industries and coalmines, which are the major sources of local emissions. The ROI-D is dominated by continental and marine aerosols, most of which can be easily detected close to their sources (He *et al.*, 2012). Overall, dust and anthropogenic pollutants often influence the columnar optical properties of aerosol in all parts of the northern YRD.

Aerosol and Cloud Properties

Cloud Optical Thickness (COT)

Fig. 2 shows the distribution of COTs varying with AODs, which are averaged over AOD size-bins (with constant bin-width: 0.02) ranging from 0.2 to 1. Clearly, COTs are notably uni-modal in the ROI-B, ROI-C and ROI-D, and almost reach to maximum at AODs of 0.6–0.74. The peaks of COTs are close to 17 in the ROI-C, ROI-D with a smaller value of 15 in the ROI-B. A possible reason is that clouds turn thicker in mountainous areas (e.g., ROI-C and ROI-D) as a result of new particles' activation (Bangert *et al.*, 2011). In contrast, COTs ascend slowly, and multimodal peaks appear in the ROI-A, such as COTs of 7.1 and 8.4 corresponding to AODs of 0.44 and 0.88, respectively.

In the ROI-A, COTs grow as aerosols increase, and particularly COTs of the clouds below 4.6 km are correlated with AODs below 0.6 (Table S1). In the ROI-B, ROI-C and ROI-D, COTs and AODs are positively-correlated at low-level AODs (< 0.6) and negatively-correlated at high-level AODs (0.6–1.0). In the ROI-B, COTs are highly sensitive to AODs, and the COTs of all height-type clouds are affected equally by AODs at low-level. As for high-clouds, the inhibiting effect of aerosol on COTs is more pronounced (R^2 = 0.47) than the promoting effect. In the ROI-C, with

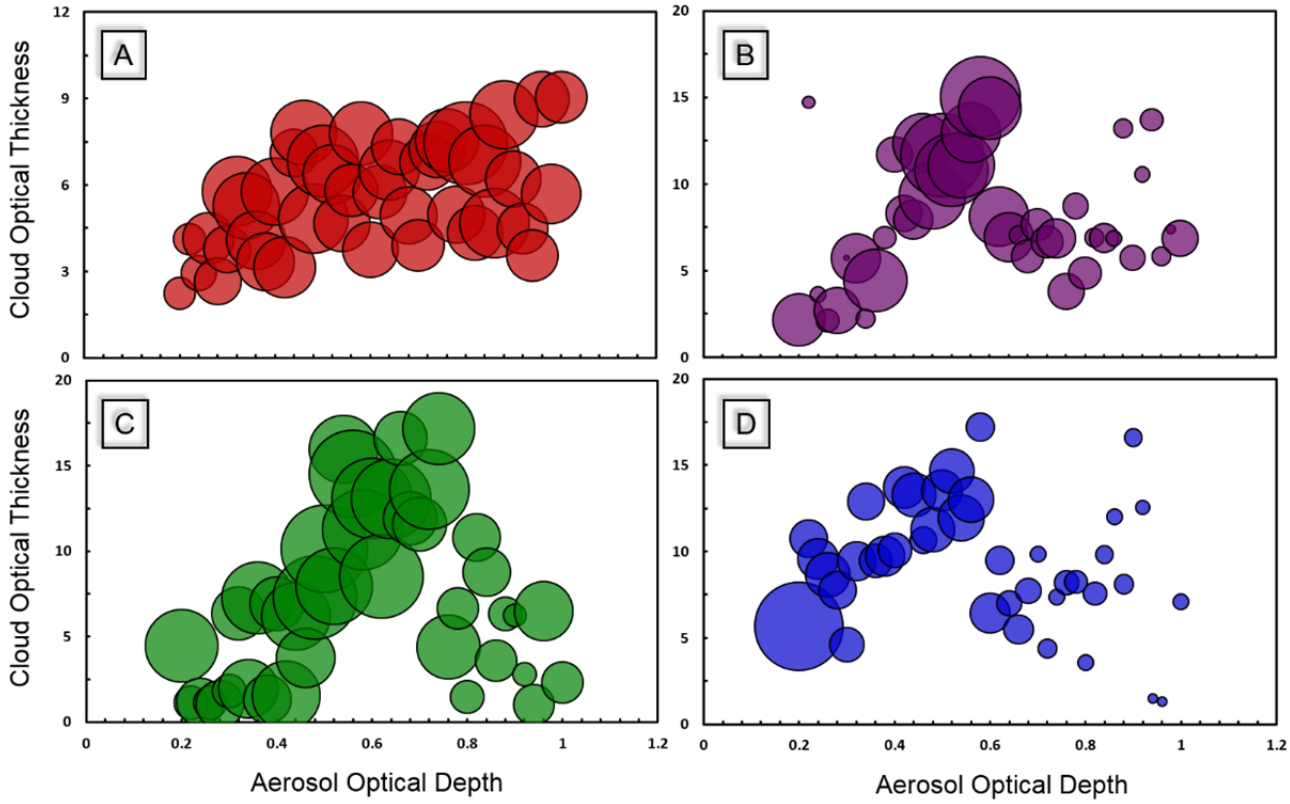

Fig. 2. Cloud optical thickness (COT) averaged over 40 AOD bins, for the four ROIs. The AOD bins are averaged for AOD size-bins of constant bin-width 0.02 over AOD ranging from 0.2 to 1. The area of the circle represents the sample number in each bin. The relationships are further quantified in Table S1.

the exception of high-clouds, the influence of low-level AODs on the COTs of other types of clouds is relatively stronger than that in the ROI-B, while high-level AODs are less influential in the ROI-B than the ROI-C and cast no evident impacts on high-clouds. In the ROI-D, COTs and AODs show a significant positive correlation at low-level AODs, for example, a steep slope in the COT/AOD relation (3.58) appears in high-clouds. Generally, COTs link closely to AODs, in particular for low- and medium-low clouds in the ROI-A, low- and high-clouds in the ROI-B and ROI-D, and all clouds except high-clouds in the ROI-C.

Cloud Liquid Water Path (LWP)

The other important microphysical property of clouds is LWP. The relationships between LWPs and AODs are shown in Fig. 3. The characteristics of LWP-AOD are somewhat similar to those of COT-AOD (Fig. 2). AODs of 0.6–0.74 correspond to the peak of LWPs in the ROI-B, ROI-C and ROI-D. In the ROI-C, LWPs increase by a factor of about 14 as AODs increase from 0.22 to 0.66, which is the largest increase among these ROIs. Otherwise, in the ROI-A, although LWPs grow smoothly with AODs on the whole, no distinct peaks are detected, and the content of column air water increases by 425% as AODs increase from 0.2 to 0.96. The growth rate of LWPs in the ROI-A is similar to that of the ROI-B, but the promoting effects of AOD on LWP are quite different for these two zones (0.2–1 vs. 0.2–0.6). This discrepancy is likely due to the presence of a large amount of non-hygroscopic aerosols in the ROI-A (Liu and Wang, 2010).

Generally, LWPs increase with AODs when AODs are at low levels in the four ROIs. LWPs and AODs are negative-correlated at high-level AODs in the ROI-B, ROI-C and ROI-D, but weakly positive-correlated in the ROI-A. Specifically, in the ROI-A, the promotion of the aerosol positive effect slows down with growing cloud height and increasing AOD. Although aerosol plays equal roles in all height-type clouds in the ROI-B, the best-fit slopes at high-level AODs are twice as large as those at low-level AODs, and correlation coefficients for the clouds below 4.6 km are larger than for clouds in higher layers (Table S1). In other words, for each level of clouds, LWPs increase slowly (AOD < 0.6) but decrease sharply (AOD > 0.6) with increasing AODs. In contrast to the ROI-B, the promoting effect of AODs on LWPs in the ROI-C at low AODs is marked, while the inhibiting effect is not significant at high AODs (Table S1). In addition, the promoting effect on low clouds in the ROI-C is the most pronounced. In the ROI-D, the pronounced effect of AODs on LWPs is mainly found on low- and high-clouds at low-level AODs (Table S1). In particular, the LWP/AOD best-fit slope of high-clouds, such as 2.53 at low-level AODs and –3.46 at high-level AODs, is much higher than that of other height-type clouds.

Many studies have also displayed the correlation of LWPs and AODs in other regions of the world. For instance, a report over Pakistan (Alam *et al.*, 2010), where aerosol is

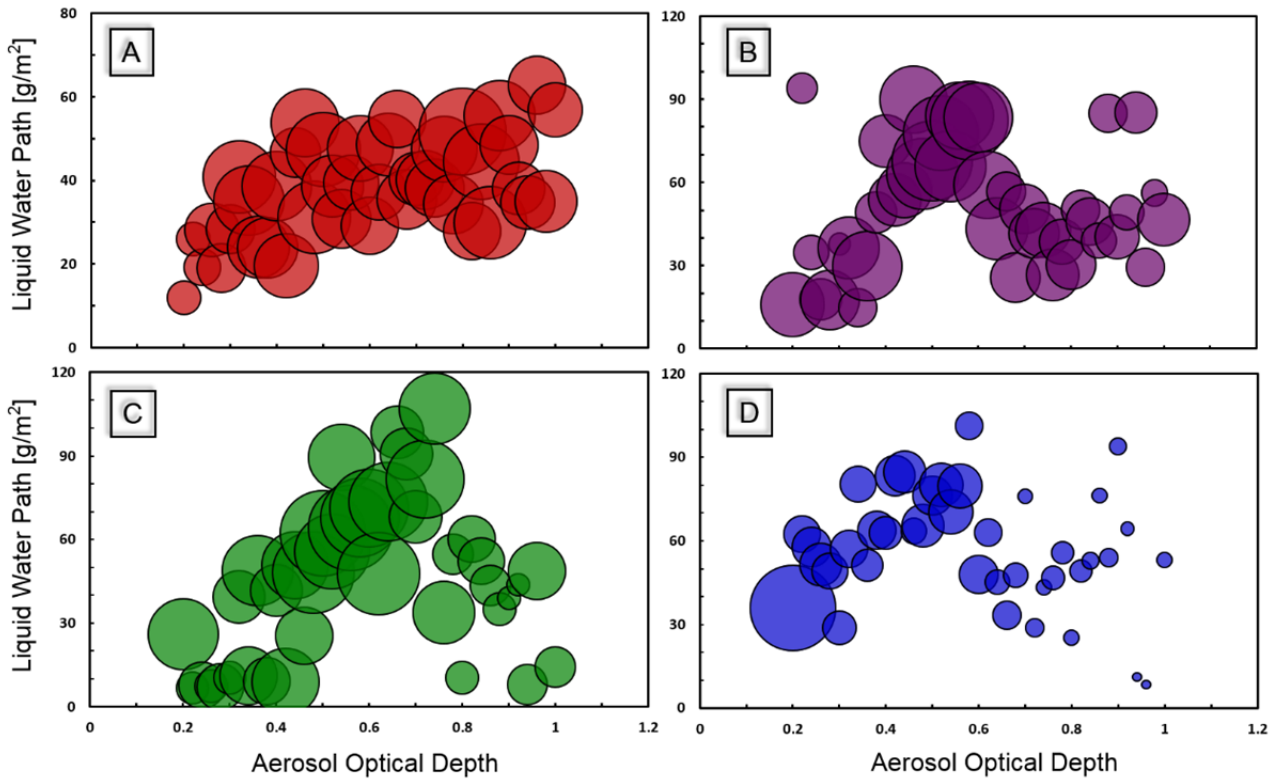

Fig. 3. Same as Fig. 2, but for liquid water path (LWP).

dominated by coarse particles, is similar to our results of the ROI-A, where positive correlations of LWP-AOD are found mainly due to their common seasonal patterns. LWPs play an important role in AIE (L'Ecuyer *et al.*, 2009), and the findings confirm that high-aerosol conditions tend to decrease LWPs, and the magnitude of LWP reduction is greater in the unstable environment of non-precipitating clouds (Lebsock *et al.*, 2008). Moreover, the fact that increasing LWPs are not systematically associated with increasing AODs (Fig. 3) indicates there is no definite relationship between AODs and LWPs.

Cloud Droplet Radius (CDR)

Fig. 4 presents the relationship between CDR and AOD by calculating the mean CDRs averaged for AOD size-bins with constant bin-width (0.02). The results show that CDRs vary between 9.5 μm and 11 μm in all ROIs. For the ROI-A, two sections indicate weak positive correlation between CDRs and AODs. For the ROI-B, however, it is of negative correlation for these two sections. As for the ROI-C and ROI-D, CDRs exhibit a similar pattern showing CDR decreases as AODs increase at low-levels, and a consistent CDR increase at high-levels. Therefore, CDRs show an insignificant dependence on AODs (Table S1). As a whole, CDRs show little exponential dependence on AODs, consequently, the simple exponential presentation cannot easily reflect their complex relationship.

There exists a functional relationship between COT, CDR, LWP (Costantino *et al.*, 2013) and the variations of COT and CDR are sensitive to LWP. Therefore, in order to understand AOD-CDR, cloud height and LWP are controlled to evaluate their potential impacts on clouds of different height-type by calculating correlation coefficients of cloud parameters (e.g., CDR, LWP, COT) (Table S1). Firstly, it is notable that a considerable proportion of relatively high correlation coefficients mostly occur in low clouds. Fig. 5 shows total cloud and aerosol occurrence frequencies below 10 km over the entire YRD. The cloud frequencies are multimodal, ranging from 93% around 1 km to 26% around 10 km, among which most cases exceeding 50% obviously occur at the low (< 3 km) and high (6–9 km) layers. As for aerosol layer fraction, we find that high frequency occurs for altitudes below 3.6 km ASL (above sea level), with maximum frequency around 1.2 km, and the frequency then decreases to zero with increasing height. Overall, both cloud and aerosol most frequently appear below 3 km, indicating that low cloud (altitude from the surface to 2.8 km) plays an important role in AIE within each ROI. Therefore, we use 3-h average data of low-cloud from CERES in the following analyses.

We divide LWPs into six grades for analysis of CDR changes with AODs. In Fig. 6, CDRs present different tendencies as AOD changes at different levels of LWP. When LWPs are low (i.e., thin cloud, LWP < 50 g m^{-2}), CDRs increase gradually with AODs. The CDRs in the ROI-A and ROI-B increase with AODs synchronously at LWPs of 50–100, but decrease in the ROI-C and ROI-D. Overall, it indicates that for a mountainous area with abundant column water, an inhibiting effect of AOD on CDR appears as the aerosol loading increases. When LWP is growing, however, the relationship of CDR with AODs turns ambiguous.

Meanwhile, some of the CDRs show a clearly decreasing tendency with LWPs at constant AODs under LWP < 200 g m^{-2}, such as for higher AODs (AOD > 0.6) in the ROI-D and for medium aerosol loading (0.4 < AOD < 0.6) in the ROI-B. Conversely, for LWP > 200 g m^{-2}, there are no obvious changes with growing LWPs because of limited data. This can be contrasted to an increasing tendency that has been observed in the Amazon because of different meteorological and biosphere conditions (Yu *et al.*, 2007; Michibata *et al.*, 2014).

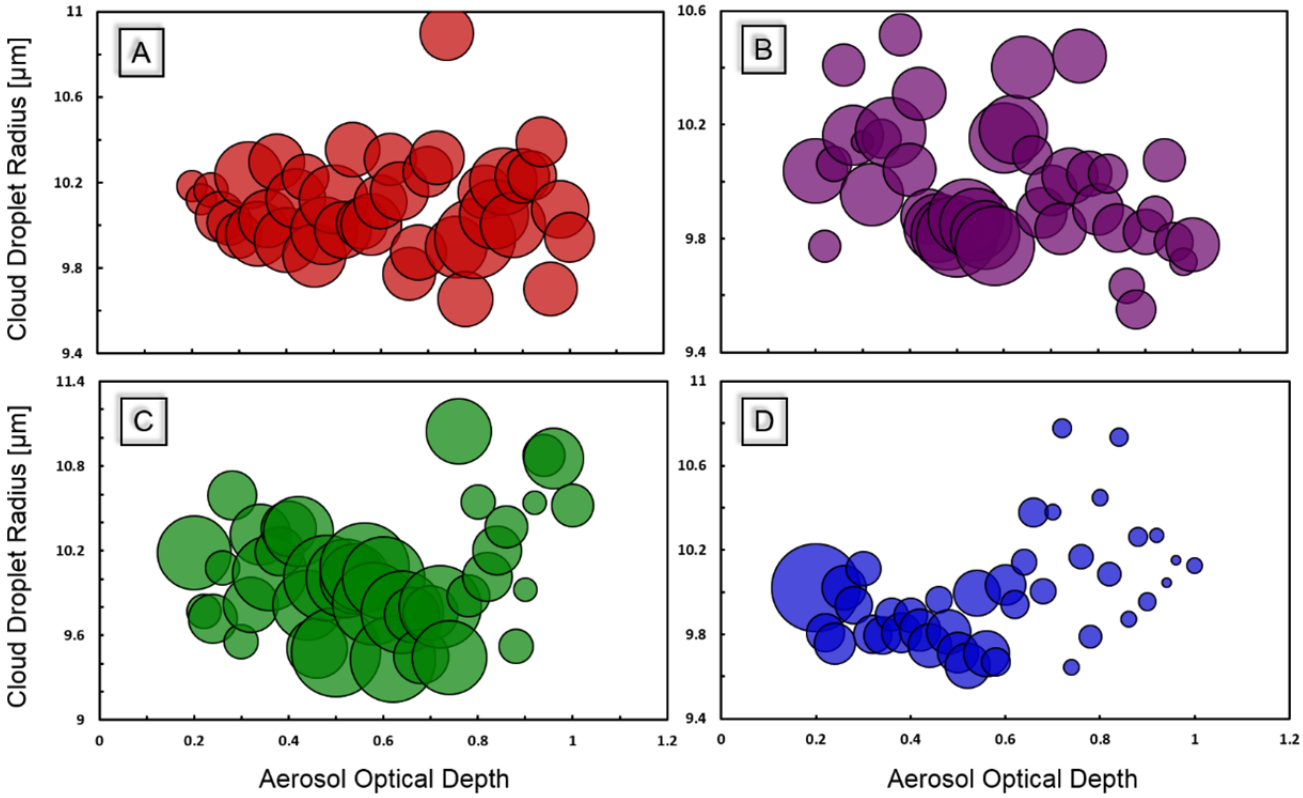

Fig. 4. Same as Fig. 2, but for cloud droplet radius (CDR).

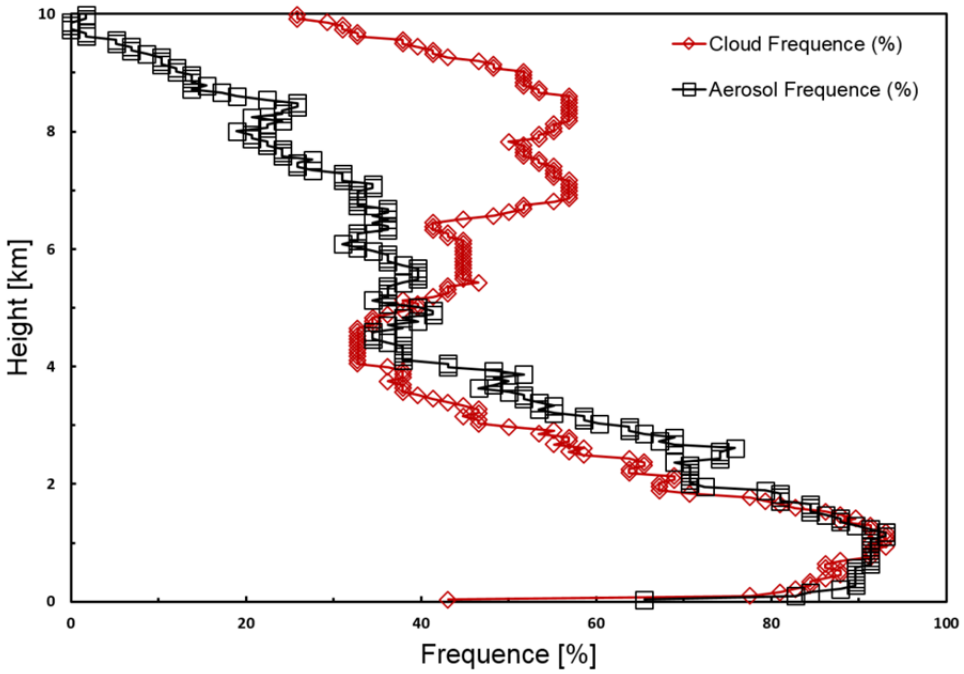

Fig. 5. Profiles of total cloud and aerosol frequencies below 10 km derived from cloud/aerosol layer fraction data.

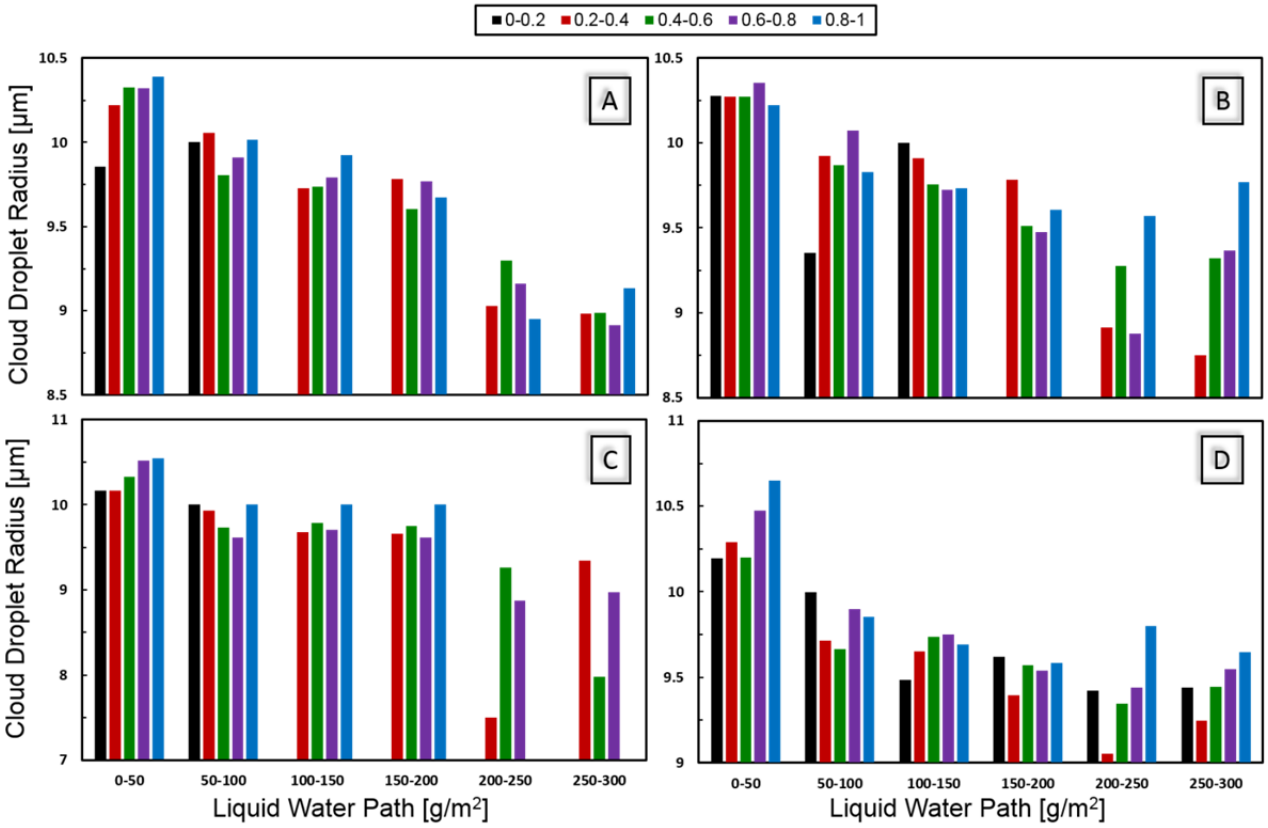

Fig. 6. The cloud droplet radius (CDR) distribution of three-hourly mean low-cloud according to AOD and LWP over four ROI. Colors present different levels of AOD from 0 to 1.

In this study, we use AOD/LWP to reflect the proportion of aerosol and water content. Fig. 7 shows COTs and CDRs averaged over a constant size-bin width (0.1) of AOD/LWP in log-log scale, in which AODs are adjusted to LWPs of the same magnitude. COTs decrease with AOD/LWP, while CDRs increase with it in all the ROIs. However, the ranges of COT, CDR, and AOD/LWP values are changeable in different ROIs. In the ROI-A, the AOD/LWP maximum (15) is larger than that of the other ROIs, indicating a polluted-dry condition. Correspondingly, COTs decrease from 22.8 toward 0.6 with AOD/LWP and show a strong correlation with it. Nevertheless, the weakest tendency (–0.84) indicates that the inhibiting effect on COTs is not as strong as other ROIs. For the clear-wet ROI-D, COTs are larger than those in the ROI-A at same AOD/LWP values. Also, CDRs vary between 9 and 11, showing a weak dependence on AOD/LWP (Fig. 7). Many studies have revealed other factors on CDR variation, such as functions of different aerosol components and cloud physical dynamics (Sardina *et al.*, 2015; Chen *et al.*, 2016).

Furthermore, the relationship between aerosol and precipitation is complex as well. The increase in aerosol may reduce CDR, thus, precipitation will be inhibited under dry conditions. For humid regions or seasons, however, the more particles, the more frequently it is going to rain. Therefore, factors of seasons and locations cannot be neglected.

Obviously, precipitation is seasonally and regionally different under various aerosol loadings. Thus, we divide the YRD into four ROIs as aforementioned during wintertime, and *a* is defined as a slight pollution status (AOD < 0.5) and *b* as a severe pollution status (AOD > 0.5) (Fig. 8). If it is severely polluted in the ROI-A, it rains much more frequently, whereas the frequency of precipitation does not differ too much in the ROI-B and ROI-C under different pollution levels. Furthermore, it rains much more heavily in a more severely polluted situation, illustrating that aerosols present a promoting effect on precipitation in the north and central YDR. In an area of severe pollution, the ROI-A experiences a large proportion of high AODs, explaining the reason for particularly high precipitation frequency. Conversely, both frequency and amounts of precipitation under the condition of low AODs are greater than those under the condition of high AODs in the ROI-D, presenting a negative effect of AODs on precipitation. The discrepancy between the ROI-A and ROI-D is possibly due to different dominant aerosol types, leading to different conversion rates (from cloud water to rainwater) (Sorooshian *et al.*, 2013). The amount of precipitation increases slowly at low CDR of 10–15 μm but rapidly at higher values of 15–25 μm (Michibata *et al.*, 2014). Since there are few CDRs of high values in the study, the low frequency of large rain events becomes explanatory. On the whole, the result is in agreement with Sorooshian *et al.* (2009), who believe that clouds with low LWP (< 500 g m^{-2}) generate little rain and are not strongly susceptible to precipitation due to aerosol.

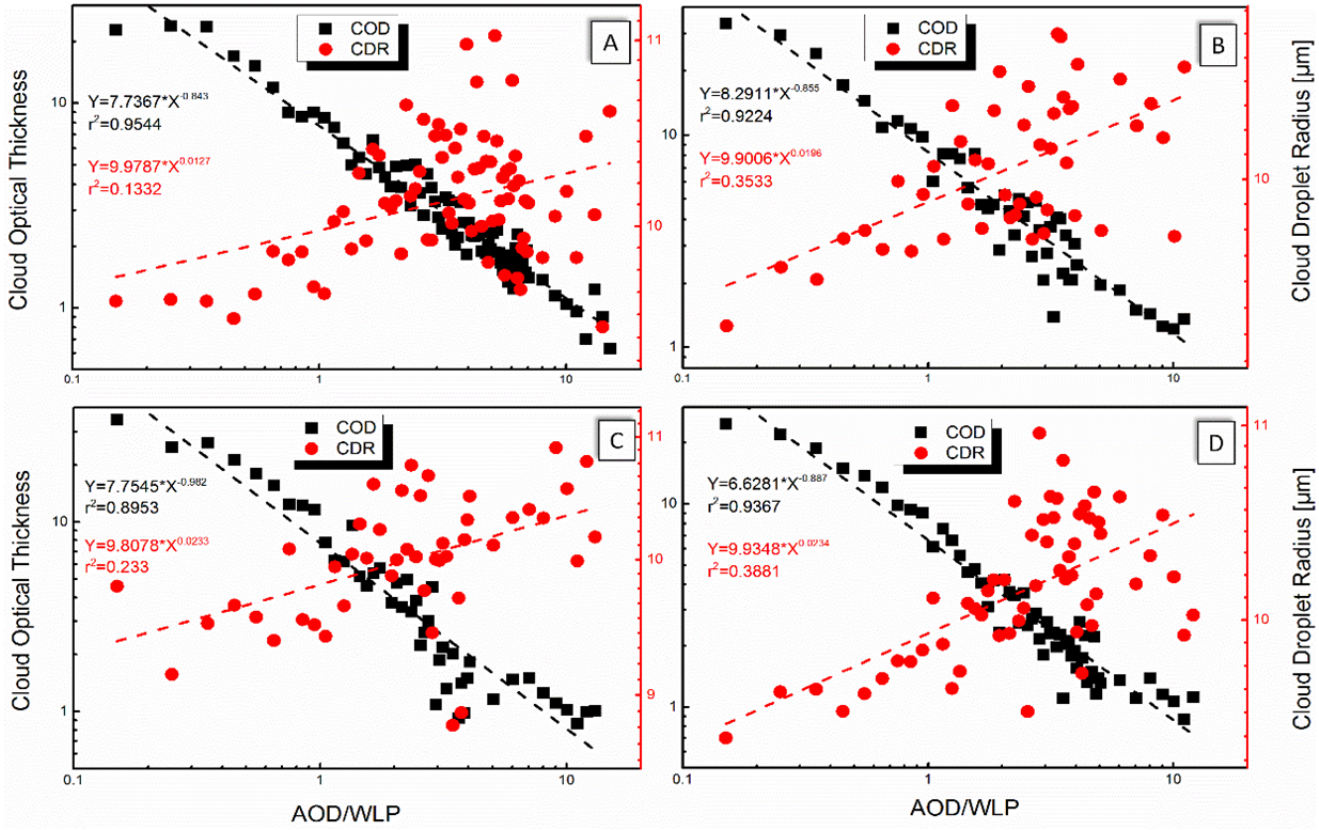

Fig. 7. Over the four ROIs, cloud optical thickness (COT) and cloud droplet radius (CDR) averaged over AOD/LWP bins with constant size-bin width (0.1) in log-log scale, in which AODs are adjusted to LWPs by same magnitude.

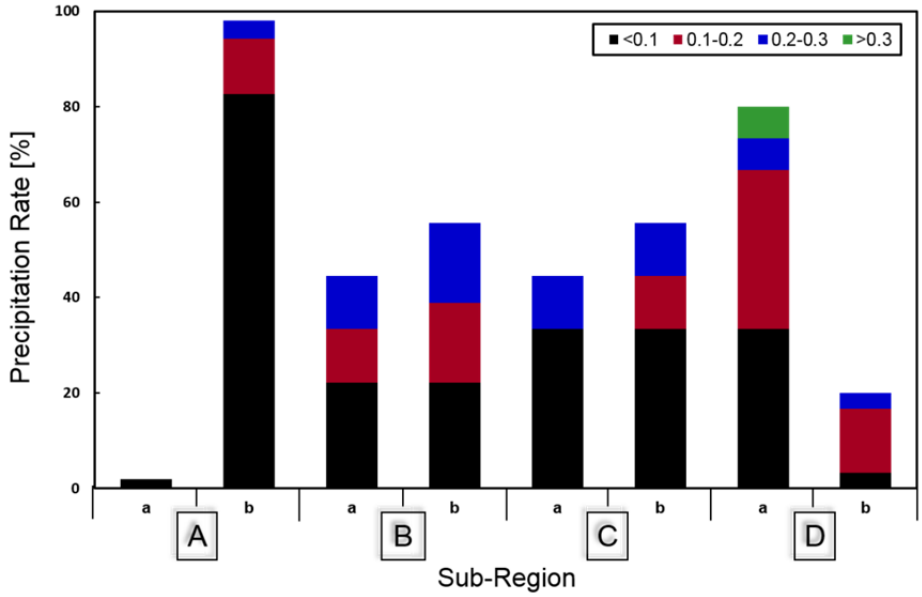

Fig. 8. Frequency of precipitation amount under clean and polluted conditions in four ROI. Colors show different precipitation amount (mm). The *a* and *b* in x-coordinate indicate AOD < 0.5 and > 0.5, respectively.

Cloud Fraction (CF)

Cloud top pressure (CTP) can roughly imply cloud vertical development. Its role in AOD-CF interactions has been investigated in previous studies of eastern Asia (Alam *et al.*, 2014; Wang *et al.*, 2014). Moreover, the hygroscopicity of aerosol and meteorological and climatic conditions exert strong influences in aerosol–cloud interactions as well (Gryspeerdt *et al.*, 2014). In this study, AODs dominantly drive the variation of CTPs over all the ROIs, irrespective of the pressure system and water amount (Figs. 9 and 10).

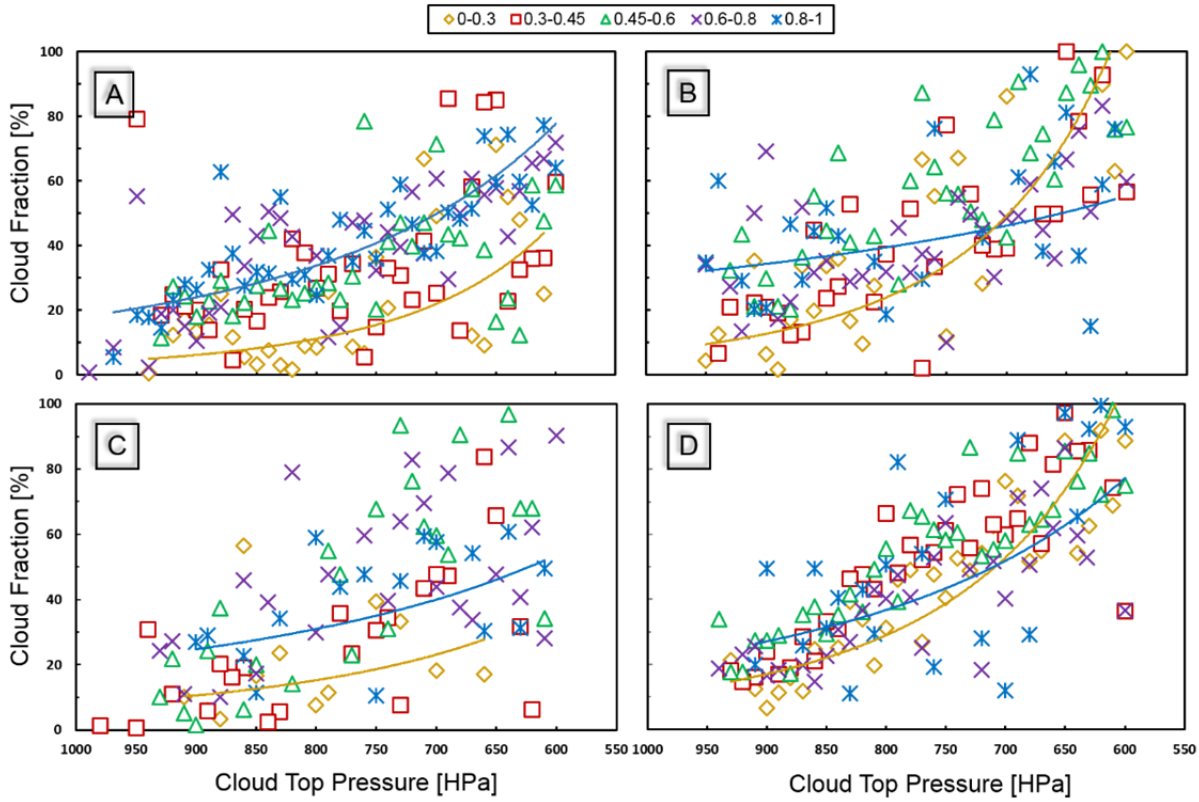

Fig. 9. CLF-CTP relationships from CERES-SYN daily products in four sub-region. The whole dataset is sorted as low to high polluted atmospheres by AOD at interval of 0.2.

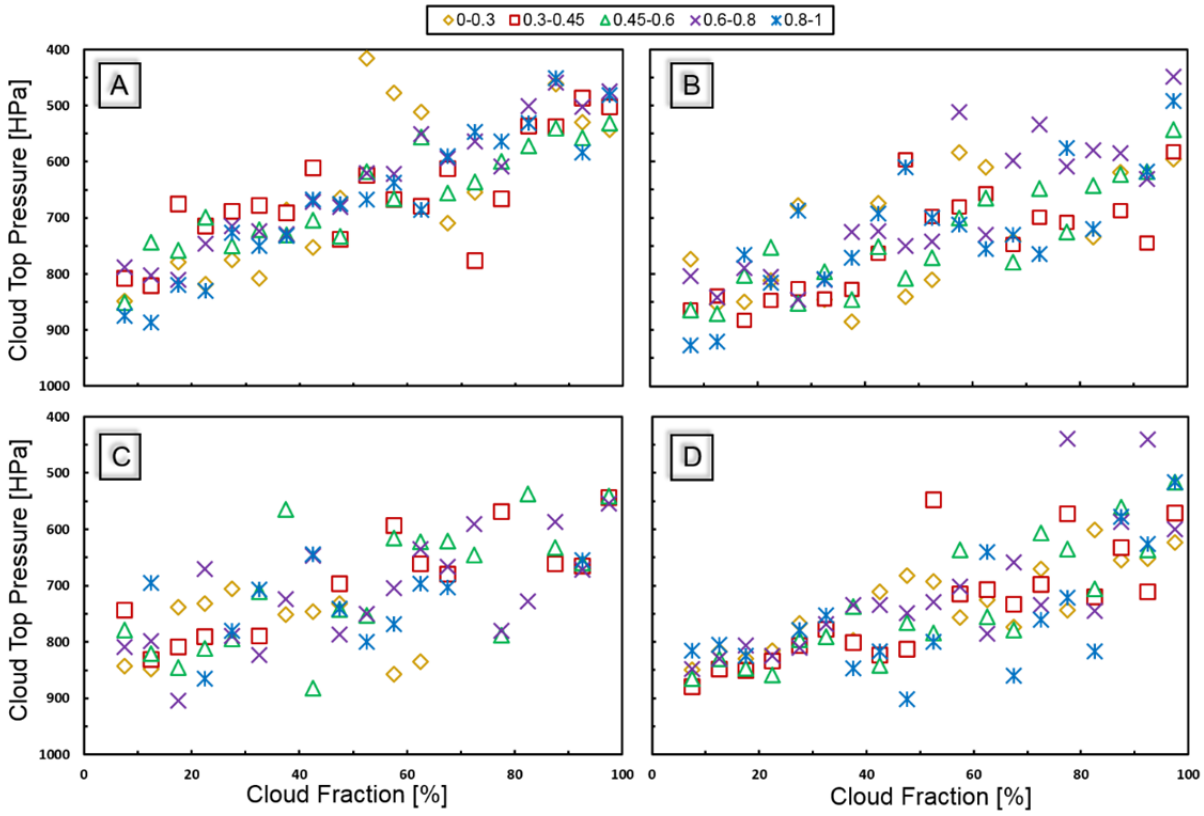

Fig. 10. CTP-CLF relationships from CERES-SYN daily products in four ROI. The whole dataset is sorted as low to high polluted atmospheres by AOD at interval of 0.2.

Fig. 9 shows a scatter plot of daily averaged CFs and CTPs in the four ROIs at different AODs. CERES daily product data is also sorted into five categories based on AODs at a constant size-bin interval of 0.2. We draw two trend lines of different aerosol loadings, the yellow one is for a data subset of 0–0.3 and the blue one is for a subset of 0.8–1. Notably, in the ROI-A and ROI-C, the cloud coverages under the conditions of high-level AODs are generally larger than those under the conditions of low-level AODs. There often exist positive relationships between AODs and CFs even considering water vapor and synoptic variability (Kourtidis *et al.*, 2015). Compared with the ROI-A and ROI-C, the lower AODs of the ROI-B and ROI-D not only have more remarkably positive effects on cloud evolvement, but also possess larger cloud fraction if CTPs are less than 700 hPa.

Meanwhile, Fig. 10 shows CTPs exhibit small differences with AODs among the four ROIs. CF-CTP under the conditions of different AODs is almost cumulatively distributed in one line in the ROI-A, as well as in the ROI-D when the CF < 40%. With regard to the ROI-B, ROI-C and ROI-D (CF > 40%), high-level AODs are not always associated with small CTPs, suggesting that aerosol-cloud interaction do not lead to the variations of CTPs. A possible reason is that aerosols influence the horizontal extension of clouds rather than the vertical distribution (Costantino *et al.*, 2013).

Aerosol Types and Low Clouds

In fact, most aerosol particles are found in the low atmosphere for stagnant atmospheric conditions during wintertime. To explore relationships between cloud parameters and aerosol types (Table 2), we analyze low clouds due to ample amounts of clouds and aerosols appearing at low altitudes as previously described (Jones *et al.*, 2009).

Although dust accounts for a large proportion of AODs, marine and continental aerosols exert notable effects on COTs and LWPs in all the ROIs except ROI-A. It is mainly because dust, as a poorly hygroscopic aerosol, is less likely to be mixed with water vapor and become CCN. Marine aerosols, comprising both organic and inorganic components from primary and secondary sources, have equal impacts on COTs and LWPs in the ROI-C and ROI-D, and furthermore, thicken the clouds. Nevertheless, dust aerosols have just slight impacts on COTs and LWPs in the ROI-A. It is likely that dust particles can be coated with hygroscopic material (i.e., sulfate) in polluted regions, greatly increasing their ability to act as effective CCN (Satheesh *et al.*, 2006; Karydis *et al.*, 2011).

The correlation coefficients, as for CDRs, between different aerosol types are close. It is worth noting that negative values of K (best-fit slope) only appear in marine aerosols of the ROI-B and continental aerosols of the ROI-A, ROI-B and ROI-D. In other words, CDRs decrease along with increasing marine or continental aerosols in the ROI-B and continental aerosol in the ROI-A and ROI-D. Additionally, small values of the correlation coefficients (R^2) demonstrate that a precise analysis is difficult to achieve if only aerosol types are taken into consideration.

Polluted Aerosol and Clouds Development: A Detailed Case Study

Fig. 11 shows the daily averages of AODs from 26 January to 8 February, covering both the growing and mitigating process of one pollution event over the YRD. High AODs are mainly found across a large domain, involving Shanghai, Anhui Province, northeastern Jiangxi Province, southern and western Jiangsu Province, and northwestern Zhejiang Province on 27 January. From then onwards, the polluted areas gradually reduce to Shanghai and Jiangsu Province only, up to 2 February. Clearly, AODs increase from 27 January to 1 February in the north of Jiangsu Province, but decrease from 2 to 8 February. The traditional Chinese New Year is just within this period.

In order to understand aerosol and cloud vertical distributions during the above-mentioned period, frequency profiles of aerosol and cloud were calculated by layer fraction from CALIPSO daily data below 10 km in the region of (31–36°E, 117–122°N). The results are shown in Fig. 12, where four days are chosen as a case study and the aerosol and cloud layer data comes from CALIPSO. Fig. 12 highlights that aerosol reaches high frequency (> 70%)

Table 2. AOD-COT, AOD-LWP, AOD-CDR relationships from MODIS daily products of low cloud in four sub-regions (K is best-fit slope). The whole dataset is sorted as aerosol types based on combined AOD and FMF retrievals.

		Marine aerosol		Dust aerosol		Continental aerosol	
		K	R^2	K	R^2	K	R^2
COT	A	0.1369	0.0034	0.737	0.2978	0.159	0.0101
	B	0.6997	0.4683	0.2815	0.0395	0.444	0.143
	C	1.9429	0.6261	0.4079	0.0211	1.4507	0.4518
	D	1.4804	0.5924	0.2767	0.0478	0.9948	0.2586
LWP	A	0.1754	0.0055	0.6547	0.261	–0.028	0.0004
	B	0.622	0.4233	0.1304	0.0101	0.3177	0.0912
	C	1.9564	0.6332	0.494	0.037	1.3061	0.4106
	D	1.4118	0.5847	0.223	0.0386	0.8059	0.2114
CDR	A	0.0744	0.1846	0.0392	0.1896	–0.039	0.1348
	B	–0.011	0.0113	0.0129	0.038	–0.027	0.0587
	C	0.0109	0.0248	0.0688	0.0969	0.0108	0.0049
	D	0.0232	0.1116	0.0481	0.1599	–0.007	0.0058

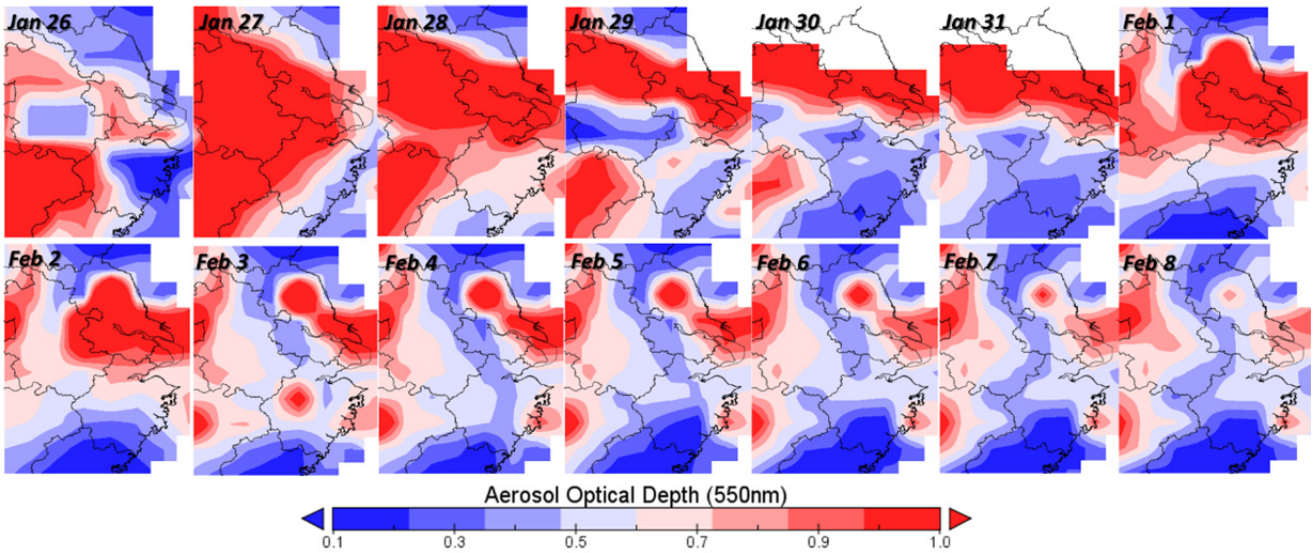

Fig. 11. Spatial distribution of daily mean AOD (0.55 μm) over the Yangtze River Delta (YRD) from 26 January to 8 February 2014.

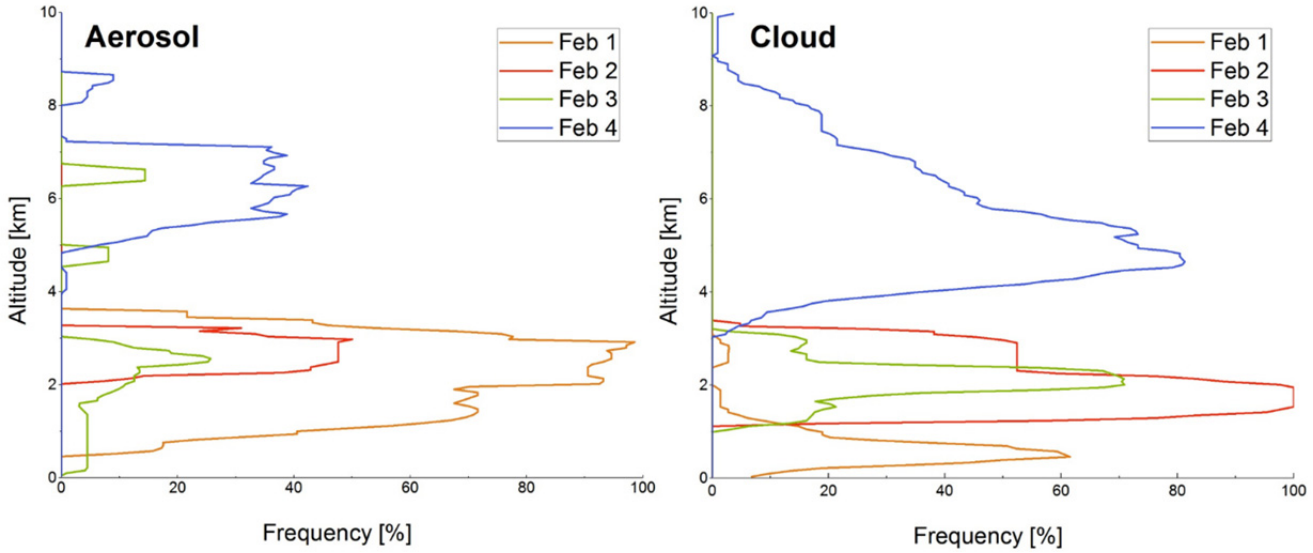

Fig. 12. Profiles of total cloud and aerosol frequencies below 10 km from CALIPSO daily data in the region of [31°–36°E, 117°–122°N].

between the height of 1.2 and 3 km on 1 February (brown line). Meanwhile, cloud layers develop from relatively low occurrence frequency (< 60%) below a height of 1 km on 1 February to high frequency (the maximum reaches 100%) between the height of 1.2 and 3 km on 2 February. With a major decline in aerosol at the same altitude on 2 and 3 February, the frequency of cloud occurrence at the height of 2.5 km clearly deceases by nearly 30% on 3 February. Furthermore, it can be noticed that peaks in the aerosol occurrence frequency occur at higher altitudes, around 4.8 km and 6.5 km on 3 February as well as 5.6 to 7 km on 4 February. Correspondingly, the clouds develop in the vertical.

The daily averages of surface lifted index (SLI), sea level pressure (SLP) and $PM_{2.5}$ concentrations are shown in Fig. 13. The SLI, calculated by temperature at the surface and 500 hPa, is applied to indicate the stability status of the atmosphere. The SLI and SLP are smaller on 1 and 2 February than the other days. It shows that the air mass moves relatively weakly in the vertical direction. Aerosol shows a reduction, as the aerosol frequency decreases from the 1st to the 2nd at the same altitude under these stable atmosphere conditions. Taking into account the lifetime of aerosol and its action time on cloud, the cloud on 2 February may well be the result of the 1 February aerosol effect.

The time series of SLI variation displays a sharp increase during three days (from 2 to 4 February). In addition, the SLP > 1008 hPa represents the core of high-pressure systems and ascending motions of air. The synoptic system with an increasing SLP demonstrates that the air mass ascends during these days. The concentration of $PM_{2.5}$ sharply

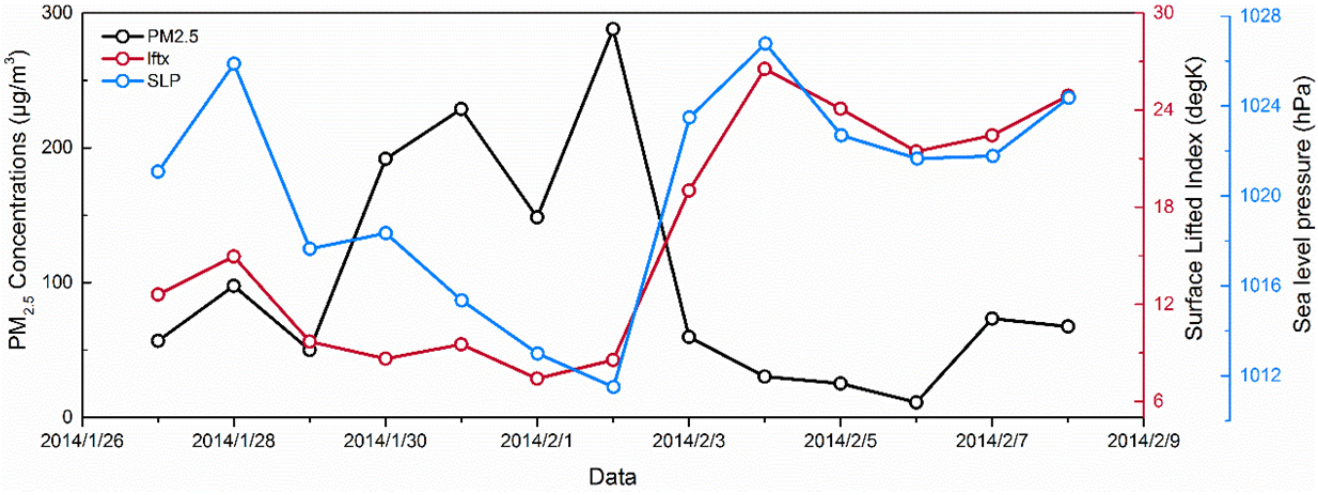

Fig. 13. Daily averages of $PM_{2.5}$, surface lifted index (SLI) and sea-level pressure (SLP) in region (31°–36°E, 117°–122°N) from 27 January to 8 February 2016. The $PM_{2.5}$ data come from the on-line monitoring and analysis platform for air quality in China (http://www.aqistudy.cn), while the SLI and SLP are from NCEP reanalysis data.

declines from 288 μg m^{-3} to 30.5 μg m^{-3}, that is coincident with air mass updrafts and horizontal transport. Accordingly, aerosols start to appear in the upper atmosphere, such as at 4.8 km and 6.5 km on 3 February and 5 to 9 km on 4 February. At the same time, a peak in the cloud frequency appears at higher altitude on the 3 February and the cloud is only distributed between 3 and 9 km on 4 February. This phenomenon shows the cloud distribution varies with the vertical distribution of aerosol.

In addition, to identify the horizontal advection and vertical distribution of aerosol and cloud layers, the air mass forward trajectories matrix from NOAA's HYSPLIT model are shown in Fig. 14(a), starting on 2 February and at 150-m height. Most of these forward trajectories show that aerosols are transported to the southwest at first. Then blue lines at two locations (33.5°E–119.5°N, 33.5°E–122°N) direct to the northeast, while the air mass flows back and is elevated to 3500 m or higher on 4 February. In contrast, backward trajectories at 6500-m height on 4 February (Fig. 14(b)), take air horizontal and vertical movements into consideration. With a sharp decline of low-cloud fraction and unremarkable variation of high-cloud parameters (Fig. 16), it can be inferred that the enhanced high-cloud fraction is mainly caused by transport. In other words, the occurrence of high aerosol layer on 4 February is mainly caused by vertical elevation of air masses from the polluted near-ground levels and long-distance horizontal transportation from the west.

Air mass transportation has great influences on aerosol micro-properties (e.g., particle size, shape, composition) and consequently clouds development. For example, smoke and polluted dust occur on 1 February (Fig. 15) below the height of 3 km. There are significant influences on the size distribution and chemical composition of aerosols mixed with dust and polluted particles (Wang *et al.*, 2007; Sun *et al.*, 2010), particularly smoke (Ackerman *et al.*, 2003). The polluted aerosol is likely to be produced by fireworks during the Spring Festival. Additionally, the YRD is an area with significant black carbon (Streets *et al.*, 2001; Bond *et al.*, 2004) and sulfate (Akimoto *et al.*, 1994; Streets *et al.*, 2000; Lu *et al.*, 2010) emissions. Thus, dust particles in this aerosol mass can be coated with water-soluble materials so can easily evolve into CCN. Moreover, an evident increase in cloud amount (Fig. 12), is very similar to the results shown by Yu *et al.* (2007), with a decrease of CDRs and an increase of COTs appearing in adjacent clouds (low- and mid-low clouds) on the following day (2 February). These factors amplify the cooling effect at the surface and the top of atmosphere (TOA), consequently, the relatively stable atmosphere appears at low altitude. With the low values of SLI and SLP (Fig. 13), large concentrations of $PM_{2.5}$ remain at ground level during these two days. The atmosphere suddenly becomes unstable from 3 February (Fig. 13) as AODs and aerosol layer fractions decrease on 2 February. Also, as shown in Fig. 16, from 4 to 7 February, LWPs of low- and mid-low clouds increase systemically from noon to midnight. Under these conditions, a greater content of column water and stronger air updraft could reduce the critical super-saturation for droplet growth and relatively favor the activation of aerosol particles into CCN, hence, more effectively decrease the droplet size (Feingold *et al.*, 2003; Kourtidis *et al.*, 2015).

CONCLUSION

The AIE during a heavily polluted winter (from December 2013 to February 2014) in the YRD was analyzed using datasets of AODs and cloud parameters obtained from CERES. Statistical analyses demonstrate that a complex relationship exists between aerosol loadings and the micro-/macro-physical parameters of clouds. Aerosol exhibits an important and complex influence on cloud evolution in the low layers of the troposphere in four typical ROIs.

The correlations of CDR-AOD, LWP-AOD and COT-AOD demonstrate that despite minor differences in the four ROIs, the AIE is in good agreement with Twomey's

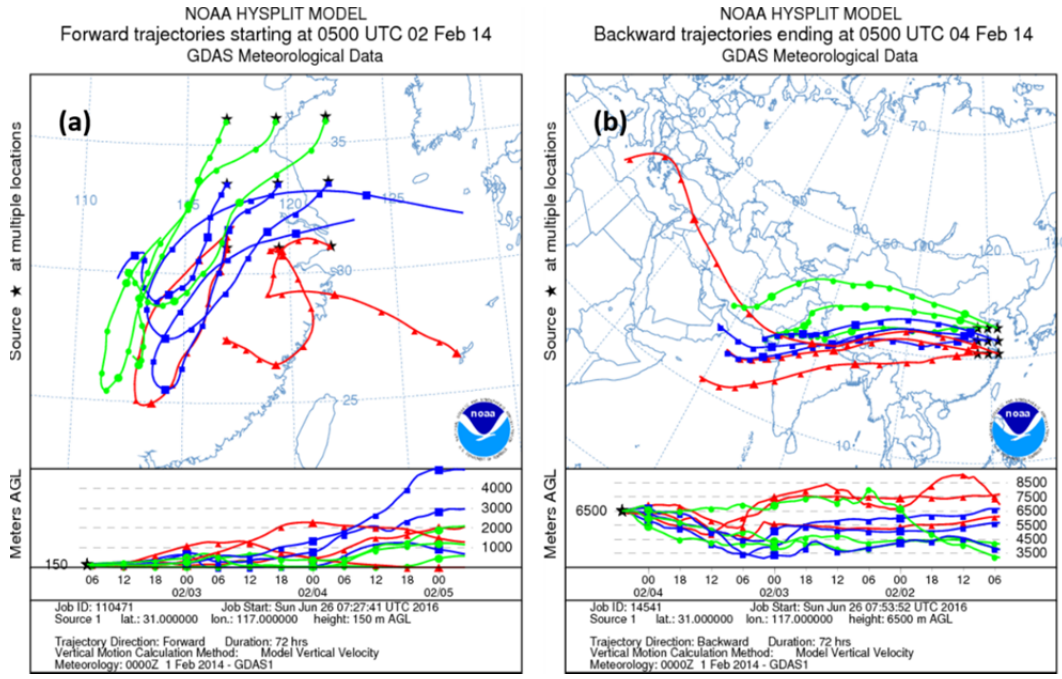

Fig. 14. Multiple sites of 3-day air mass (a) forward trajectories starting at 150 m on 2 February, (b) backward trajectories ending at 6500 m on 4 February. Those trajectories were calculated by the NOAA Hybrid Single Particle Lagrangian Trajectory (HYSPLIT) model.

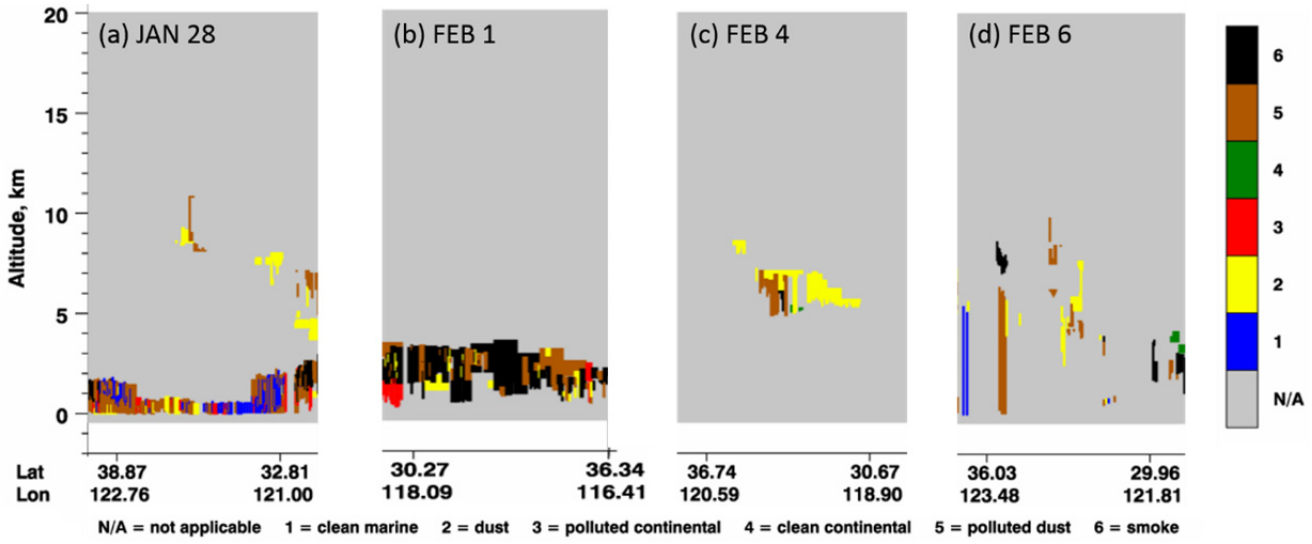

Fig. 15. Aerosol subtypes on 28 Jan., 1 Feb., 4 Feb. and 6 Feb. retrieved from CALIPSO vertical feature data.

hypothesis for low-level AODs. As the cloud height increases, the correlation between aerosol and clouds decreases, and with a stable atmosphere, the AIE mainly stays active in the low troposphere (below 5 km) during winter. Ground pollution possibly increases low cloud cover. Synoptic conditions also significantly impact cloud cover. For instance, an unstable synoptic condition causes clouds to develop to a larger horizontal extent and at higher altitudes.

In general, meteorological and geographical conditions strongly affect the cloud cover (Norris, 1998). Most studies of AIE do not contest that these parameters result in variations in the cloud quantity and properties. Airflow brings uncertainty to the assessment of AIE factors based on satellite observation. Furthermore, we need to improve our understanding of the physical and thermodynamic properties of clouds, which play an important role in cloud development but are not considered in this paper. The classifications of aerosol and clouds are still rather general and cannot accurately illustrate the relationships between aerosol types and different clouds. We highlight the profound influence of geographical factors as well as the climatic impact of aerosol, both of which require further investigation.

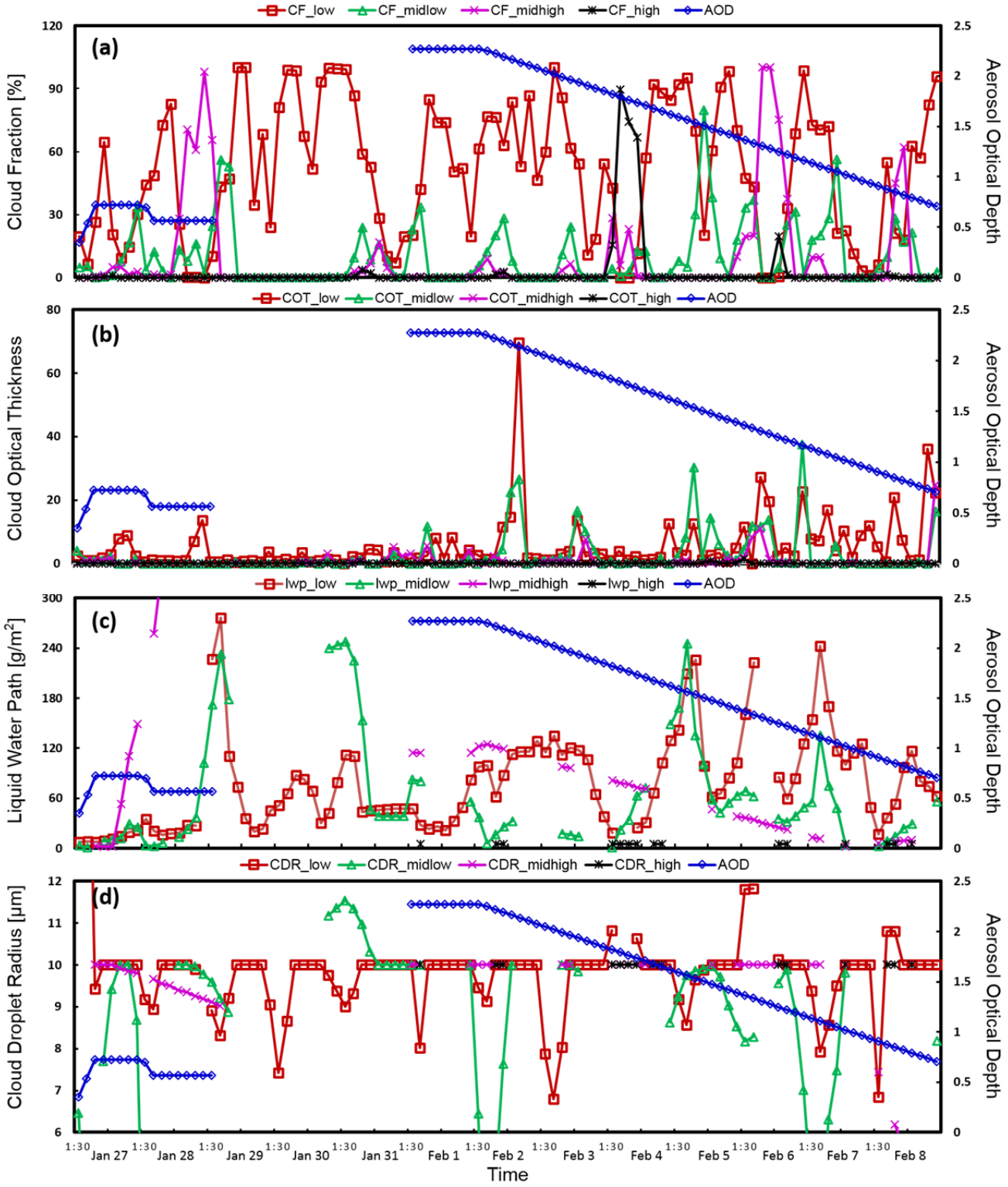

Fig. 16. Time series of cloud property parameters (CF, COT, LWP and CDR) from CERES-SYN 3-hourly data between 27 Jan. to 28 Feb. 2014. Colors represent clouds at different altitudes.

ACKNOWLEDGEMENTS

This research is supported by the National Key Research and Development Program of Ministry of Science and Technology (2016YFC0202003, 2017YFC1501405) and the National Natural Science Foundation of China (41475109, 41775129, 21577021, 21377028, 91637101) and partly supported by the Science and Technology Commission of Shanghai Municipality (16ZR1431700).

SUPPLEMENTARY MATERIAL

Supplementary data associated with this article can be found in the online version at http://www.aaqr.org.

REFERENCES

Ackerman, A.S., Toon, O.B., Stevens, D.E. and Coakley, J.A. (2003). Enhancement of cloud cover and suppression of nocturnal drizzle in stratocumulus polluted by haze. *Geophys. Res. Lett.* 30: 1381.

Ackerman, A.S., Toon, O.B., Stevens, D.E., Heymsfield, A.J., Ramanathan, V. and Welton, E.J. (2000). Reduction of tropical cloudiness by soot. *Science* 28*:* 1042–1047.

Akimoto, H. and Narita, H. (1994). Distribution of SO_2, NO_x and CO_2 emissions from fuel combustion and industrial activities in Asia with 1 × 1 resolution. *Atmos. Environ.* 28: 213–225.

Alam, K., Iqbal, M.J., Blaschke, T., Qureshi, S. and Khan, G. (2010). Monitoring spatio-temporal variations in aerosols and aerosol–cloud interactions over Pakistan using MODIS data. *Adv. Space Res.* 46: 1162–1176.

Alam, K., Khan, R., Blaschke, T. and Mukhtiar, A. (2014). Variability of aerosol optical depth and their impact on cloud properties in Pakistan. *J. Atmos. Sol. Terr. Phys.* 107: 104–112.

Albrecht, B.A. (1989). Aerosols, cloud microphysics, and fractional cloudiness. *Science* 245: 1227–1230.

Anderson, A.K. and Sobel, N. (2003). Dissociating intensity from valence as sensory inputs to emotion. *Neuron* 39: 581–583.

Bangert, M., Kottmeier, C., Vogel, B. and Vogel, H. (2011). Regional scale effects of the aerosol cloud interaction simulated with an online coupled comprehensive chemistry model. *Atmos. Chem. Phys.* 11: 4411–4423.

Barnaba, F. and Gobbi, G.P. (2004). Aerosol seasonal variability over the Mediterranean region and relative impact of maritime, continental and Saharan dust particles over the basin from MODIS data in the year 2001. *Atmos. Chem. Phys.* 4: 2367–2391.

Bond, T.C., Streets, D.G., Yarber, K.F., Nelson, S.M., Woo, J.H. and Klimont, Z. (2004). A technology-based global inventory of black and organic carbon emissions from combustion. *J. Geophys. Res.* 109: D14203.

Brenguier, J.L., Pawlowska, H. and Schüller, L. (2003). Cloud microphysical and radiative properties for parameterization and satellite monitoring of the indirect effect of aerosol on climate. *J. Geophys. Res.* 108: 8632.

Bréon, F.M., Tanré, D. and Generoso, S. (2002). Aerosol effect on cloud droplet size monitored from satellite. *Science* 295: 834–838.

Chan, C.K. and Yao, X. (2008). Air pollution in mega cities in China. *Atmos. Environ.* 42: 1–42.

Chen, S., Bartello, P., Yau, M.K., Vaillancourt, P.A. and Zwijsen, K. (2016). Cloud droplet collisions in turbulent environment: Collision statistics and parameterization. *J. Atmos. Sci.* 73: 621–636.

Costantino, L. and Bréon, F.M. (2013). Aerosol indirect effect on warm clouds over South-East Atlantic, from co-located MODIS and CALIPSO observations. *Atmos. Chem. Phys.* 13: 69–88.

Draxler, R.R. and Rolph, G.D. (2003). HYSPLIT (HYbrid Single-Particle Lagrangian Integrated Trajectory) model access via NOAA ARL READY website (http://www.arl.noaa.gov/ready/hysplit4. html). NOAA Air Resources Laboratory, Silver Spring.

Feingold, G., Eberhard, W.L., Veron, D.E. and Previdi, M. (2003). First measurements of the Twomey indirect effect using ground-based remote sensors. *Geophys. Res. Lett.* 30: 1287.

Forest, C.E., Stone, P.H., Sokolov, A.P., Allen, M.R. and Webster, M.D. (2002). Quantifying uncertainties in climate system properties with the use of recent climate observations. *Science* 295: 113–117.

Fu, X., Wang, S.X., Cheng, Z., Xing, J., Zhao, B., Wang, J.D. and Hao, J.M. (2014). Source, transport and impacts of a heavy dust event in the Yangtze River Delta, China, in 2011. *Atmos. Chem. Phys.* 14: 1239–1254.

Gryspeerdt, E., Stier, P. and Partridge, D.G. (2014). Satellite observations of cloud regime development: The role of aerosol processes. *Atmos. Chem. Phys.* 14: 1141–1158.

Guo, J., Su, T., Li, Z., Miao, Y., Li, J., Liu, H., Xu, H., Cribb, M. and Zhai, P. (2017). Declining frequency of summertime local-scale precipitation over eastern China from 1970–2010 and its potential link to aerosols. *Geophys. Res. Lett.* 44: 5700–5708.

Hansen, J., Sato, M. and Ruedy, R. (1997). Radiative forcing and climate response. *J. Geophys. Res.* 102: 6831–6864.

He, Q., Li, C., Geng, F., Lei, Y. and Li, Y. (2012). Study on long-term aerosol distribution over the land of East China using MODIS data. *Aerosol Air Qual. Res.* 12: 304–319.

Hu, Q., Fu, H., Wang, Z., Kong, L., Chen, M. and Chen, J. (2016). The variation of characteristics of individual particles during the haze evolution in the urban Shanghai atmosphere. *Atmos. Res.* 181: 95–105.

Jin, M. and Shepherd, J.M. (2008). Aerosol relationships to warm season clouds and rainfall at monthly scales over east China: Urban land versus ocean. *J. Geophys. Res.* 113: D24S90.

Jones, T.A., Christopher, S.A. and Quaas, J. (2009). A six year satellite-based assessment of the regional variations in aerosol indirect effects. *Atmos. Chem. Phys.* 9: 4091–4114.

Kalnay, E., Kanamitsu, M., Kistler, R., Collins, W., Deaven, D., Gandin, L., Iredell, M., Saha, S., White, G., Woollen, J., Zhu, Y., Chelliah, M., Ebisuzaki, W., Higgins, W., Janowiak, J., Mo, K.C., Ropelewski, C., Wang, J., Leetmaa, A., Reynolds, R., Jenne, R. and Joseph, D. (1996). The NCEP/NCAR 40-year reanalysis project. *Bull. Am. Meteorol. Soc.* 77: 437–471.

Karydis, V.A., Kumar, P., Barahona, D., Sokolik, I.N. and Nenes, A. (2011). On the effect of dust particles on global cloud condensation nuclei and cloud droplet number. *J. Geophys. Res.* 116: D23204.

Knutti, R., Stocker, T.F., Joos, F. and Plattner, G.K. (2002). Constraints on radiative forcing and future climate change from observations and climate model ensembles.

Nature 416: 719–723.

Kong, S., Li, X., Li, L., Yin, Y., Chen, K., Yuan, L., Zhang, Y., Shan, Y. and Ji, Y. (2015). Variation of polycyclic aromatic hydrocarbons in atmospheric $PM_{2.5}$ during winter haze period around 2014 Chinese Spring Festival at Nanjing: Insights of source changes, air mass direction and firework particle injection. *Sci. Total Environ.* 520: 59–72.

Kourtidis, K., Stathopoulos, S., Georgoulias, A.K., Alexandri, G. and Rapsomanikis, S. (2015). A study of the impact of synoptic weather conditions and water vapor on aerosol–cloud relationships over major urban clusters of China. *Atmos. Chem. Phys.* 15: 10955–10964.

Lebsock, M.D., Stephens, G.L. and Kummerow, C. (2008). Multisensor satellite observations of aerosol effects on warm clouds. *J. Geophys. Res.* 113: D15205.

L'Ecuyer, T.S., Berg, W., Haynes, J., Lebsock, M. and Takemura, T. (2009). Global observations of aerosol impacts on precipitation occurrence in warm maritime clouds. *J. Geophys. Res.* 114: D09211.

Leng, C., Duan, J., Xu, C., Zhang, H., Wang, Y., Wang, Y., Li, X., Kong, L., Tao, J., Zhang, R., Cheng, T., Zha, S. and Yu, X. (2016). Insights into a historic severe haze event in Shanghai: Synoptic situation, boundary layer and pollutants. *Atmos. Chem. Phys.* 16: 9221–9234.

Leng, C., Zhang, Q., Tao, J., Zhang, H., Zhang, D., Xu, C., Li, X., Kong, L., Cheng, T., Zhang, R., Yang, X., Chen, J., Qiao, L., Lou, S., Wang, H. and Chen, C. (2014). Impacts of new particle formation on aerosol cloud condensation nuclei (CCN) activity in Shanghai: Case study. *Atmos. Chem. Phys.* 14: 11353–11365.

Liu, J., Zheng, Y., Li, Z., Flynn, C. and Cribb, M. (2012). Seasonal variations of aerosol optical properties, vertical distribution and associated radiative effects in the Yangtze Delta region of China. *J. Geophys. Res.* 117: D00K38.

Liu, X. and Wang, J. (2010). How important is organic aerosol hygroscopicity to aerosol indirect forcing? *Environ. Res. Lett.* 5: 044010.

Loeb, N.G. and Manalo-Smith, N. (2005). Top-of-atmosphere direct radiative effect of aerosols over global oceans from merged CERES and MODIS observations. *J. Clim.* 18: 3506–3526.

Lohmann, U. and Feichter, J. (2005). Global indirect aerosol effects: A review. *Atmos. Chem. Phys.* 5: 715–737.

Lu, Z., Streets, D.G., Zhang, Q., Wang, S., Carmichael, G.R., Cheng, Y.F., Wei, C., Chin, M., Diehl, T. and Tan, Q. (2010). Sulfur dioxide emissions in China and sulfur trends in East Asia since 2000. *Atmos. Chem. Phys.* 10: 6311–6331.

Menon, S., Hansen, J., Nazarenko, L. and Luo, Y. (2002). Climate effects of black carbon aerosols in China and India. *Science* 297: 2250–2253.

Michibata, T., Kawamoto, K. and Takemura, T. (2014). The effects of aerosols on water cloud microphysics and macrophysics based on satellite-retrieved data over East Asia and the North Pacific. *Atmos. Chem. Phys.* 14: 11935–11948.

Minnis, P., Young, D.F., Sun-Mack, S., Heck, P.W., Doelling, D.R. and Trepte, Q.Z. (2004). CERES cloud property retrievals from imagers on TRMM, Terra, and Aqua. Proc. SPIE 5235, Remote Sensing of Clouds and the Atmosphere VIII, pp. 37–48.

Monks, P.S., Granier, C., Fuzzi, S., Stohl, A., Williams, M.L., Akimoto, H., Amann, M., Baklanov, A., Baltensperger, U., Bey, I., Blake, N., Blake, R.S., Carslaw, K., Cooper, O.R., Dentener, F., Fowler, D., Fragkou, E., Frost, G.J., Generoso, S., Ginoux, P., Grewe, V., Guenther, A., Hansson, H.C., Henne, S., Hjorth, J., Hofzumahaus, A., Huntrieser, H., Isaksen, I.S.A., Jenkin, M.E., Kaiser, J., Kanakidou, M., Klimont, Z., Kulmala, M., Laj, P., Lawrence, M.G., Lee, J.D., Liousse, C., Maione, M., McFiggans, G., Metzger, A., Mieville, A., Moussiopoulos, N., Orlando, J.J., O'Dowd, C.D., Palmer, P.I., Parrish, D.D., Petzold, A., Platt, U., Pöschl, U., Prévôt, A.S.H., Reeves, C.E., Reimann, S., Rudich, Y., Sellegri, K., Steinbrecher, R., Simpson, D., ten Brink, H., Theloke, J., van der Werf, G.R., Vautard, R., Vestreng, V., Vlachokostas, C. and von Glasow, R. (2009). Atmospheric composition change-global and regional air quality. *Atmos. Environ.* 43: 5268–5350.

Norris, J.R. (1998). Low cloud type over the ocean from surface observations. Part I: Relationship to surface meteorology and the vertical distribution of temperature and moisture. *J. Clim.* 11: 369–382.

Norris, J.R. (1998). Low cloud type over the ocean from surface observations. Part II: Geographical and seasonal variations. *J. Clim.* 11: 383–403.

Penner, J.E., Dong, X. and Chen, Y. (2004). Observational evidence of a change in radiative forcing due to the indirect aerosol effect. *Nature* 427: 231–234.

Platnick, S., King, M.D., Ackerman, S.A., Menzel, W.P., Baum, B.A., Riédi, J.C. and Frey, R.A. (2003). The MODIS cloud products: Algorithms and examples from Terra. *IEEE Trans. Geosci. Remote Sens.* 41: 459–473.

Pöschl, U. (2005). Atmospheric aerosols: Composition, transformation, climate and health effects. *Angew. Chem. Int. Ed.* 44: 7520–7540.

Quaas, J., Boucher, O. and Bréon, F.M. (2004). Aerosol indirect effects in POLDER satellite data and the Laboratoire de Météorologie Dynamique–Zoom (LMDZ) general circulation model. *J. Geophys. Res.* 109: D08205.

Ramanathan, V., Crutzen, P.J., Lelieveld, J., Mitra, A.P., Althausen, D., Anderson, J., Andreae, M.O., Cantrell, W., Cass, G.R., Chung, C.E., Clarke, A.D., Coakley, J.A., Collins, W.D., Conant, W.C., Dulac, F., Heintzenberg, J., Heymsfield, A.J., Holben, B., Howell, S., Hudson, J., Jayaraman, A., Kiehl, J.T., Krishnamurti, T.N., Lubin, D., McFarquhar, G., Novakov, T., Ogren, J.A., Podgorny, I.A., Prather, K., Priestley, K., Prospero, J.M., Quinn, P.K., Rajeev, K., Rasch, P., Rupert, S., Sadourny, R., Satheesh, S.K., Shaw, G.E., Sheridan, P. and Valero, F.P.J. (2001). Indian Ocean Experiment: An integrated analysis of the climate forcing and effects of the great Indo-Asian haze. *J. Geophys. Res.* 106: 28371–28398.

Remer, L.A. and Kaufman, Y.J. (2006). Aerosol direct radiative effect at the top of the atmosphere over cloud free ocean derived from four years of MODIS data.

Atmos. Chem. Phys. 6: 237–253.

Remer, L.A., Kaufman, Y.J., Tanré, D., Mattoo, S., Chu, D.A., Martins, J.V., Li, R.R., Ichoku, C., Levy, R.C., Kleidman, R.G., Eck, T.F., Vermote, E. and Holben, B.N. (2005). The MODIS aerosol algorithm, products, and validation. *J. Atmos. Sci.* 62: 947–973.

Rolph, G.D. (2003). Real-time environmental applications and Display sYstem (READY) Website (http://www.arl.noaa.gov/ready/hysplit4. html). NOAA Air Resources Laboratory, Silver Spring. Md.

Rosenfeld, D. (2000). Suppression of rain and snow by urban and industrial air pollution. *Science* 287: 1793–1796.

Sardina, G., Picano, F., Brandt, L. and Caballero, R. (2015). Continuous growth of droplet size variance due to condensation in turbulent clouds. *Phys. Rev. Lett.* 115: 184501.

Satheesh, S.K., Moorthy, K.K., Kaufman, Y.J. and Takemura, T. (2006). Aerosol optical depth, physical properties and radiative forcing over the Arabian Sea. *Meteorol. Atmos. Phys.* 91: 45–62.

Sorooshian, A., Feingold, G., Lebsock, M.D., Jiang, H. and Stephens, G.L. (2009). On the precipitation susceptibility of clouds to aerosol perturbations. *Geophys. Res. Lett.* 36: L13803.

Sorooshian, A., Wang, Z., Feingold, G. and L'Ecuyer, T.S. (2013). A satellite perspective on cloud water to rain water conversion rates and relationships with environmental conditions. *J. Geophys. Res.* 118: 6643–6650.

Streets, D.G. and Waldhoff, S.T. (2000). Present and future emissions of air pollutants in China: SO_2, NO_x, and CO. *Atmos. Environ.* 34: 363–374.

Streets, D.G., Gupta, S., Waldhoff, S.T., Wang, M.Q., Bond, T.C. and Yiyun, B. (2001). Black carbon emissions in China. *Atmos. Environ.* 35: 4281–4296.

Sun, Y., Zhuang, G., Huang, K., Li, J., Wang, Q., Wang, Y., Lin, Y., Fu, J.S., Zhang, W., Tang, A. and Zhao, X. (2010). Asian dust over northern China and its impact on the downstream aerosol chemistry in 2004. *J. Geophys. Res.* 115: D00K09.

Tan, C., Zhao, T., Xu, X., Liu, J., Zhang, L. and Tang, L. (2015). Climatic analysis of satellite aerosol data on variations of submicron aerosols over East China. *Atmos. Environ.* 123: 392–398.

Tang, J., Wang, P., Mickley, L.J., Xia, X., Liao, H., Yue, X., Sun, L. and Xia, J. (2014). Positive relationship between liquid cloud droplet effective radius and aerosol optical depth over Eastern China from satellite data. *Atmos. Environ.* 84: 244–253.

Twomey, S. (1974). Pollution and the planetary albedo. *Atmos. Environ.* 8: 1251–1256.

Wang, F., Guo, J., Zhang, J., Huang, J., Min, M., Chen, T., Liu, H., Deng, M. and Li, X. (2015). Multi-sensor quantification of aerosol-induced variability in warm cloud properties over eastern China. *Atmos. Environ.* 113: 1–9.

Wang, F., Guo, J., Wu, Y., Zhang, X., Deng, M., Li, X., Zhang, J. and Zhao, J. (2014). Satellite observed aerosol-induced variability in warm cloud properties under different meteorological conditions over eastern China. *Atmos. Environ.* 84: 122–132.

Wang, Y., Zhuang, G., Tang, A., Zhang, W., Sun, Y., Wang, Z. and An, Z. (2007). The evolution of chemical components of aerosols at five monitoring sites of China during dust storms. *Atmos. Environ.* 41: 1091–1106.

Wielicki, B.A., Barkstrom, B.R., Harrison, E.F., Lee, III, R.B., Louis Smith, G. and Cooper, J.E. (1996). Clouds and the Earth's Radiant Energy System (CERES): An earth observing system experiment. *Bull. Am. Meteorol. Soc.* 77: 853–868.

Winker, D.M., Pelon, J., Coakley, J.A., Ackerman, S.A., Charlson, R.J., Colarco, P.R., Flamant, P., Fu, Q., Hoff, R.M., Kittaka, C., Kubar, T.L., Le Treut, H., McCormick, M.P., Mégie, G., Poole, L., Powell, K., Trepte, C., Vaughan, M.A. and Wielicki, B.A. (2010). The CALIPSO mission: A global 3D view of aerosols and clouds. *Bull. Am. Meteorol. Soc.* 91: 1211–1230.

Winker, D.M., Vaughan, M.A., Omar, A., Hu, Y., Powell, K.A., Liu, Z., Hunt, W.H. and Young, S.A. (2009). Overview of the CALIPSO mission and CALIOP data processing algorithms. *J. Atmos. Oceanic Technol.* 26: 2310–2323.

Wolf, M.E. and Hidy, G.M. (1997). Aerosols and climate: Anthropogenic emissions and trends for 50 years. *J. Geophys. Res.* 102: 11113–11121.

Xia, X., Li, Z., Holben, B., Wang, P., Eck, T., Chen, H., Cribb, M. and Zhao, Y. (2007). Aerosol optical properties and radiative effects in the Yangtze Delta region of China. *J. Geophys. Res.* 112: D22S12.

Xin, J., Wang, Y., Li, Z., Wang, P., Hao, W.M., Nordgren, B.L., Wang, S., Liu, G., Wang, L., Wen, T., Sun, Y. and Hu, B. (2007). Aerosol optical depth (AOD) and Ångström exponent of aerosols observed by the Chinese Sun Hazemeter Network from August 2004 to September 2005. *J. Geophys. Res.* 112: D05203.

Xu, J., Bergin, M.H., Greenwald, R. and Russell, P.B. (2003). Direct aerosol radiative forcing in the Yangtze delta region of China: Observation and model estimation. *J. Geophys. Res.* 108: 4060.

Yu, H., Fu, R., Dickinson, R.E., Zhang, Y., Chen, M. and Wang, H. (2007). Interannual variability of smoke and warm cloud relationships in the Amazon as inferred from MODIS retrievals. *Remote. Sens. Environ.* 111: 435–449.

Zhao, C., Tie, X. and Lin, Y. (2006). A possible positive feedback of reduction of precipitation and increase in aerosols over eastern central China. *Geophys. Res. Lett.* 33: L11814.

Received for review, October 7, 2017
Revised, February 2, 2018
Accepted, April 3, 2018